

Neck fragmentation reaction mechanism

V. Baran^{a,b} M. Colonna^a M. Di Toro^a

^a*Laboratori Nazionali del Sud INFN, I-95123 Catania, Italy
Physics & Astronomy Dept., Univ. of Catania*

^b*NIPNE-HH and Physics Faculty, University of Bucharest, Romania*

Based on a microscopic transport model, we study the origin of nonstatistical Intermediate Mass Fragment (*IMF*) production in semicentral heavy ion collisions at the Fermi energies. We show that a fast, dynamical *IMF* formation process, the *neck fragmentation mechanism*, can explain the experimentally observed features: deviations from Viola systematics and anisotropic, narrow angular distributions. It may be regarded as the continuation of the multifragmentation mechanism towards intermediate impact parameters. Its relation to other dynamical mechanisms, the induced fission and the abrasion of the spectator zones, that can also contribute to mid-rapidity *IMF* production, is discussed. The dependence on beam energy and centrality of the collision is carefully analysed. The competition between volume and surface instabilities makes this mechanism very sensitive to the in-medium nucleon-nucleon interactions, from the cross sections for hard collisions to the compressibility and other Equation of State (*EOS*) properties. For charge asymmetric collisions the sensitivity of various observables to the symmetry energy is investigated. Of particular interest appears the isospin diffusion dynamics with no signal of isospin equilibration. However, in spite of the short time scales and of the dynamical aspects, we notice isoscaling features of the neck mechanism. We observe that isospin enrichment of the neck zone as well as the isoscaling parameters are sensitive to the density dependence of asymmetry term of *EOS* around and below saturation value.

Key words: Neck fragmentation; Dynamical fission; Symmetry energy; Isospin diffusion; Isoscaling.

PACS numbers: 21.30.Fe, 25.70.-z, 25.70.Lm, 25.70.Pq.

1 INTRODUCTION

The Fermi energy domain is the transition region between a dynamics driven by the mean-field, below $15 - 20 \text{ AMeV}$, and one where the nucleon-nucleon collisions play a central role, above 100 AMeV . It is the place of the rise and/or fall of new reaction mechanisms, including a liquid-gas like phase transition. Consequently it still attracts considerable theoretical and experimental efforts. One of its distinctive particularities is the enhanced production of Intermediate Mass Fragments ($IMF, 3 < Z < 21$). Their characteristics are essential to assert which dissipation mechanisms act at these energies as well as in establishing the equilibration time hierarchy of various degrees of freedom.

In particular, along the last decade, several experiments have been devoted to a better understanding of the origin of IMF 's in semi-central heavy-ion collisions at bombarding energies between 20 and $80 - 100 \text{ AMeV}$. From peripheral to semi-central collisions it has been established that the reaction mechanism has a mainly binary character and the statistical decay products from highly excited projectile-like (PLF^*) and targetlike (TLF^*) are the first to be considered in a consistent description. However, experimental evidences for IMF ' production not directly related to the statistical decay of PLF or TLF were accumulated in the past [1], [2], [3], [4] and with the advent of 4π arrays generations a more systematic analysis has been possible [5], [6], [7], [8], [9], [10], [11]. Consequently some definite particularities of this "dynamical" IMF production have been established:

- a clear enhanced emission is localized in the mid-rapidity region, intermediate between PLF and TLF rapidities, especially for fragments with charge Z from 3 to 12;
- the IMF 's relative velocity distributions with respect to PLF (or TLF) cannot be explained in terms of pure Coulomb repulsion following a statistical decay. A high degree of decoupling from the PLF (TLF) is also invoked.
- clear anisotropic IMF 's angular distributions are indicating preferential emission directions and an alignment tendency;
- for charge asymmetric systems the light particles and IMF emissions keep track of a neutron enrichment process that takes place in the neck region.

However, a fully consistent physical picture of the processes that can reproduce observed characteristics is still a matter of debate and several physical phenomena are taken into account.

One is the formation of a transient, necklike structure, joining projectile-like (PLF) and target-like (TLF). Its noncompactness, a large surface to volume

ratio, was supposed to favor fragment emission. The creation of a cylindrical geometry can trigger the Rayleigh instabilities which, as it happens in the low energy fission, will drive a multiple neck rupture. The early decoupling of this structure may explain qualitatively the observed trends.

A fission like mechanism can also be included in the discussion. Indeed, after the interaction stage, an outgoing primary nucleus, *PLF*- and/or *TLF*-like, strongly deformed and highly excited can follow a fast fission, dynamically induced, path. A prefragment with a given energy above the barrier may form on its deformed side. This will explain the observed deviations from Viola systematics. An aligned emission, due to a shorter life before scission, is also predicted.

It is possible that with increasing bombarding energy an abrasion-ablation process manifests as a precursor to the participant-spectator scenario present at higher energies. This process will induce a third decaying hot zone that amplifies the mid-rapidity fragment production. Related to this, we may refer also to the recently extended Goldhaber clustering model, allowing mixing of projectile and target nucleons and including hard-scattered nucleons from Pauli-allowed collisions, [12].

Even statistical decay of a hot source at intermediate energy, triggered by the proximity configuration with *PLF* and *TLF*, was claimed [13]. Finally we have to remind that dynamical transport models suggest since long time the possibility of such phenomena [14], [15], [3,4].

It has to be remarked that various aspects of the somehow idealized presented scenarios, do not exclude each other but they can contribute to various stages of the reaction dynamics. Moreover, the weak points of each explanation must not be neglected:

- In applying the Rayleigh stability criteria, it has to be realized that neck matter is not incompressible, but it can be warmed up and expanded. The matching of the reaction time at these energies, much shorter than in low energy fission, with the growth time-scale of Rayleigh instabilities [16] could be also a problem.
- In a dynamical fission scenario, having in mind the strong dissipation towards the scission point, the question raises about the possibility for the prefragment to have enough energy to escape with the velocity needed for reproducing the largest deviation from Viola systematics.
- The manifestation of a shearing off (sudden abrasion) process at lower energies is certainly largely suppressed in a slower evolution towards separation.
- Finally, the time scales for binary reactions at Fermi energies may not be large enough to allow for a consistent statistical approach to dinuclear-like and proximity adiabatic configurations, in fast continuous evolution due to

centrifugal motion of the *PLF* and *TLF* spectators.

Therefore a unified and more systematic theoretical investigation of the processes that develop in this energy range in semiperipheral collisions is required. It is certain that the intricate interplay between effects related to mean-field and direct nucleon hard collisions has to be properly described as well as the entrance channel far from equilibrium regime. A reliable possible framework is provided by a stochastic mean field microscopic approach. We consider a Boltzmann-Nordheim-Vlasov, (*BNV*), type transport model, which guarantees a good description of the mean field dynamics, we believe important for the physics in the Fermi energy range. It also includes a collision integral term that consistently accounts for the Pauli blocking. Moreover, the related fluctuations effects are considered through a stochastic procedure, as detailed below.

Based on this approach, we investigate how a fast fragment production mechanism can raise in semiperipheral collisions at intermediate energies and we try to characterize the most significant observables. We explore the conditions that promote its manifestation as well as the dependence on mean field properties and direct nucleon-nucleon collisions. In this way we will be able to suggest the optimal experimental selections (colliding ions, centrality, beam energies) for the observation of this new dissipation reaction mechanism and also to extract some fundamental information on the nuclear interaction in the medium.

We will strongly exploit the latter point in relation to isospin effects in reactions with large charge asymmetry. A peculiar attention will be payed to the transport properties of the isovector part of the equation of state (*asy*–*EOS*).

Several recent works were focused on the role of isospin and charge equilibration in mid-peripheral collisions around Fermi energies [17], [18], [19], [20], [21].

We predict that some neck-observables are sensitive to the poorly known density dependence of symmetry term of *EOS* allowing to discriminate among various proposed parametrisations. Therefore, very often in the following, our results will be presented as a comparison between different *asy*–*EOS*. Moreover, once the isospin dynamics is better understood, the fragment isospin composition can be considered as a useful marker for the physical processes that take place at different time-space regions during the reaction evolution. We expect this physics to be largely produced in the coming years at the new Radioactive Ion Beam (*RIB*) facilities in the Fermi energy domain, e.g. see ref. [22].

In our quantitative evaluations we are focusing here mainly on the neutron rich, mass asymmetric reaction $^{124}\text{Sn} + ^{64}\text{Ni}$, at 35AMeV bombarding en-

ergy, but attention has been paid also to the corresponding neutron poor reaction $^{112}\text{Sn} + ^{58}\text{Ni}$, for the reason which will become clear below. These reactions have been experimentally studied within the *REVERSE* experiment at *LNS*, Catania [23]. In spite of the low isospin densities reached with stable asymmetric beams we will be able to see interesting symmetry effects in some selected observables very sensitive to the isospin dynamics.

Based on these considerations we organize our work as follows. In Section II the main ingredients of the considered transport model are first briefly discussed. Then we present global features of the reaction dynamics for semiperipheral collisions. The density contour plots allow to identify several stages of the collision and to extract the corresponding time scales. A classification of the observed events is emerging. We identify a fast *IMF* production mechanism related to the neck dynamics which is generically called *neck fragmentation* and study its evolution with the impact parameter.

In section III we survey the kinematical properties of the *IMF*'s resulting from neck fragmentation (Neck Originating Fragments, *NOF*), including the velocity and angular distributions, for different *asy - EOS* effective forces.

In section IV, in order to better grasp the physical process leading to this mechanism, we explore the influence of compressibility and nucleon-nucleon cross sections on the neck dynamics. We underline the essential role of volume instabilities in the neck fragmentation process.

In section V we focus on the isospin dynamics in this mechanism and point out that isotopic composition of *NOF*'s as well as the clearly evinced isoscaling parameters are quite sensitive to the density dependence of the used *asy - EOS*.

The emerging picture from our study and the main results are summarized in the Conclusions, section VI.

2 SEMIPHERIPERAL COLLISIONS AROUND FERMI ENERGY: NECK FRAGMENTATION

2.1 Stochastic transport model - basic ingredients

A new code for the solution of microscopic transport equations of Boltzmann-Nordheim-Vlasov (*BNV*) type has been written where the dynamics of fluctuations is included [24]. The transport equations are solved following a test particle evolution on a lattice [25,26]. In the collision term a parameterization

of free NN cross sections is used, with energy and angular dependence. The isospin effects on the nucleon cross section and Pauli blocking are consistently evaluated. The influence of in-medium reduced cross sections is studied in Sect.IV.

We also adopt another approach to stochastic terms, computationally much easier [27,28], based on the introduction of density fluctuations by a random sampling of the phase space. The amplitude of the noise is gauged to reproduce the dynamics of the most unstable modes [28]. For each system we have checked the equivalence of the two methods in the description of the collision dynamics, from fast particle emissions to the fragment production.

Our results are first discussed considering a “soft” effective interaction, corresponding to a compressibility modulus $K = 200\text{MeV}$, see ref.[29]. In the section IV a hard EOS parametrization with $K = 380\text{MeV}$ will be also considered.

Regarding the isovector part of the EOS , three different parametrizations for the density dependence of symmetry term are adopted, the so called *asysoft*, *asystiff* and *superasystiff* *asy*– EOS , ref.[29]. We will refer to a “asystiff” EOS when the potential symmetry term linearly increases with nuclear density, to a “asysoft” EOS when the symmetry term shows saturation and eventually a decrease above normal density [30], and to a “asysuperstiff” behaviour if it has a parabolic rise with density [31,32].

To achieve a reasonable statistics, for each impact parameter and mean-field parameterization, 400 events were obtained arriving at an overall total of more than 8000 events. The BNV transport code was run until freeze-out time, when the resulted fragments are quite far apart from each other, under the action of only Coulomb repulsion. In order to select the test particles belonging to a given fragment a fast method, based on cuts in density, was considered. We have also confronted it with other methods, based on the interparticle relative distance criteria, obtaining similar results. The mass, charge, angular momentum, quadrupole and octupole deformations, excitation energies as well as CM positions and momenta for each fragment have been then evaluated.

Once the freeze-out space/momentum configuration has been fixed the Coulombian trajectories of all fragments were calculated in order to generate the asymptotic angular and velocity distributions.

2.2 Typical events and time scales

Our simulations indicate that from semicentral to peripheral collisions, above the impact parameter $b = 4fm$, i.e. $b_{red} \equiv b/b_{max} \geq 0.37$, the reaction

$^{124}\text{Sn} + ^{64}\text{Ni}$, at 35AMeV , has a mainly binary character. Based on density contour plots, as well as from multiplicities and quadrupole/octupole fragment deformations we can divide the events at freeze-out in three main classes as follows:

a) binary events, with excited Target-like and Projectile-like fragments ($TLLF^*$, $PLLF^*$) showing small deformations and therefore likely to remain so for long times; their sequential decay can be described by statistical models with reliable inputs for angular momentum and excitation energy;

b) binary events, but $PLLF^*$ and/or $TLLF^*$ acquire large quadrupole or/and octupole deformation (especially $PLLF^*$). These primary fragments now are expected to follow a dynamically induced fission-like path, faster than a pure statistical one;

c) ternary events, with a IMF directly emitted in less than 250-300 fm/c from the reaction beginning. The remaining $PLLF^*$ and $TLLF^*$'s are now in general less deformed. At the considered energy, events with two or more IMF 's appear very rare (see the discussion of Section IV).

As we have already mentioned the events of class b) can also contribute to the “dynamical” production of IMF 's we are studying here. We show in Figure 1 the scatter plot of freeze-out quadrupole versus octupole moments, ($qua = \sum_{i=1}^A(2z_i^2 - y_i^2 - x_i^2)/A$, $oct = \sum_{i=1}^A[5z_i^3 - 3z_i(x_i^2 + y_i^2 + z_i^2)]/A$), for all fragments produced in the events of classes a) and b), for two asy-parameterizations. The large dynamically induced deformations can drive especially the $PLLF^*$'s towards a fast asymmetric fission. We recognize in the figure the two branches associated to $PLLF^*$ (left) and to $TLLF^*$ (right) respectively. The corresponding signs suggest pearshaped fragments oriented with the smaller deformation towards the separation point. Unfortunately the mounting numerical inaccuracy of the transport simulations cannot allow us to follow such events up to the scission point.

Our approach will allow a detailed and quantitative analysis for only the class c) of events. Nevertheless, based on the features of this fast IMF emission mechanism, we will trace some conclusions also about the dynamically induced fission expected to involve somehow longer time scales.

We show in Figure 2 the density contour plot, projected on the reaction plane, of a typical ternary event belonging to the class c), for $b = 6\text{fm}$. Calculations are performed using the asy-stiff parameterization. For the first 20 – 40 fm/c from the touching time, the two participants deeply interact and some compression takes place. The system heats up and a relative expansion follows. In spite of its compact shape it still behaves as a two-center object and we notice that a superimposed separate motion of the PL and TL pre-fragments is effective. It induces the formation of a neck-like structure with a fast chang-

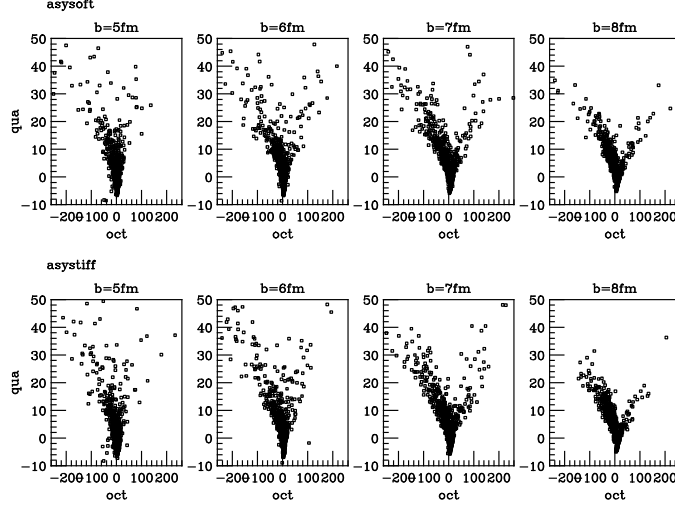


Fig. 1. Quadrupole (*qua*) versus octupole (*oct*) deformations of the fragments belonging to the event classes a) and b), see text.

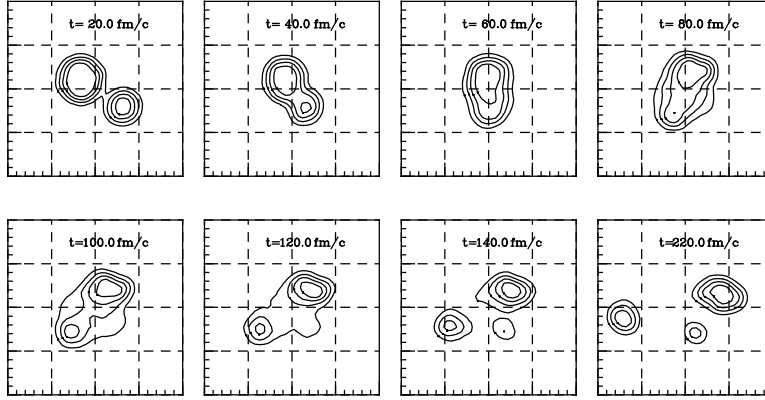


Fig. 2. Typical evolution of the density contour plot for a ternary event at $b = 6\text{fm}$ for the reaction $^{124}\text{Sn} + ^{64}\text{Ni}$ at 35AMeV .

ing geometry, between $40\text{fm}/c$ and $140 - 160\text{fm}/c$, depending on the impact parameter.

This particular neck-instability dynamics favours the appearance of *IMF*'s, after about $150\text{fm}/c$, in a variety of places and ways as can be seen by looking at Figure 3. Here, we have selected, for four events, two characteristic times, the early phase of fragment formation process and the configuration close to freeze-out. We call the *IMF*'s produced by such a mechanism Neck Origination Fragments (*NOF*'s).

We can introduce the ternary event probability as the ratio, $N_{\text{ternary}}/N_{\text{total}}$, between the number of events of class c) and the total number of events, $N_{\text{total}} = 400$ for each impact parameter. It shows an interesting dependence on the impact parameter, see Fig. 4. Its maximum, around 25%, is attained around mid-centrality, between $b = 6-7\text{fm}$. The *NOF* production probability

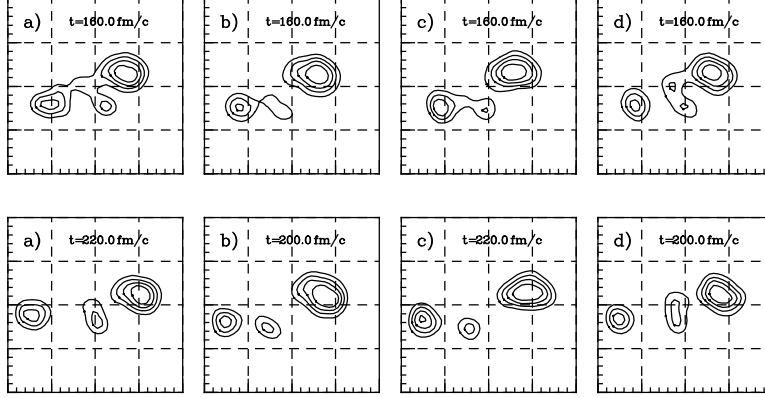


Fig. 3. Configurations corresponding to an early stage of fragment formation (top) and close to the freeze-out (bottom) for four ternary events a), b), c), d) observed in neck fragmentation at $b = 6 \text{ fm}$.

is then decreasing on both sides arriving at 10% for $b = 5 \text{ fm}$ and $b = 8 \text{ fm}$. It becomes still smaller at $b = 4 \text{ fm}$, in spite of a stronger dissipation. At variance, at larger impact parameters, $b = 9 \text{ fm}$, a less overlapping and a faster separation are also suppressing this mechanism. The trend and the corresponding values at each impact parameter are not sensibly influenced when other *asy* - *EOS* are considered and therefore we do not include the results in Fig. 4. We will show later that the isospin diffusion, i.e. the isospin content of the *NOFs*, is much more sensitive to the symmetry term of the used effective forces.

The probabilities are reduced of about 25% for the neutron poor reaction $^{112}\text{Sn} + ^{58}\text{Ni}$, (black points). We note that a similar difference in *IMF* yields between neutron poor and neutron rich systems was observed experimentally in multifragmentation events for central collisions [33]. As we shall see in the Section IV, neck fragmentation probabilities depend strongly on the the nucleon-nucleon cross sections and compressibility. All these results seem to indicate the relevance of volume instabilities even for the dynamics of neck fragmentation.

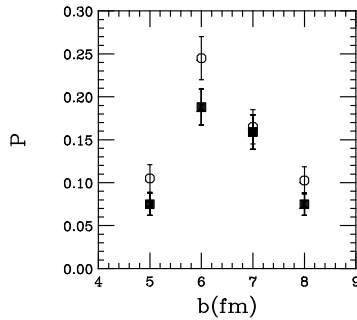


Fig. 4. The impact parameter dependence of the probability for ternary events. White circles: neutron rich reaction. Black circles: neutron poor reaction. Asystiff *EOS*.

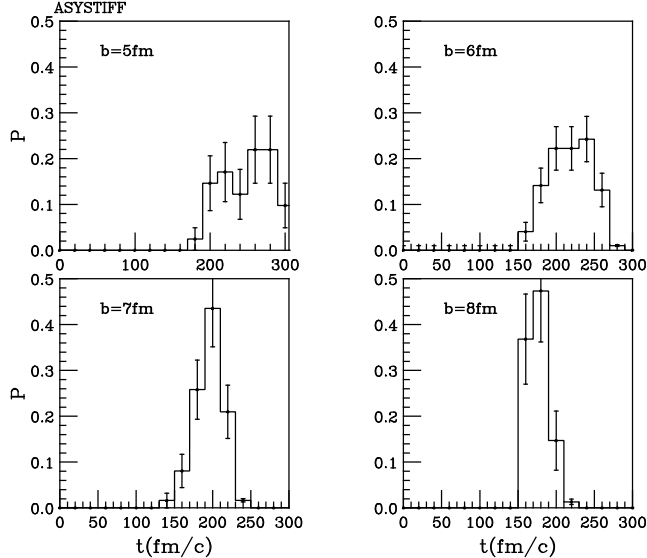


Fig. 5. NOF production rate for impact parameters from $b = 5fm$ to $8fm$ and asystiff EOS .

More insight on the NOF production mechanism is gained looking at the time dependence of the emission probability. At each $20fm/c$ we can scrutinize the density distributions searching for the appearance of new ternary events. The corresponding emission probability is obtained as the ratio between the new ternary events, identified within the specific time interval, and the total number of ternary events counted at freeze-out. From Fig. 5 we see that the NOF 's production is a fast process, taking place between $120fm/c$ and $280fm/c$, depending on impact parameter. We remind that in our initialization geometry the touching time is around $20fm/c$, see Fig.2. One can notice that the distribution becomes sharper and peaked at smaller times with increasing impact parameter, as expected.

The primary NOF 's at the freeze-out time are characterized by reduced masses and charges reflecting specific spatial and temporal constraints. The mass asymmetry distributions with respect to the PLF/TLF are shown in Figure6. We define $etp \equiv (M_{PLF} - M_{NOF})/(M_{PLF} + M_{NOF})$ and $ett \equiv (M_{TLF} - M_{NOF})/(M_{TLF} + M_{NOF})$. As expected smaller NOF 's are in general produced at larger impact parameters. We note that in this inverse kinematics reaction the smaller target mass gives a wider mass asymmetry distribution for the $TLF - NOF$ system. The mass asymmetry distribution of the fast produced NOF 's is much sharper with respect to the projectile-like fragments, with a very clear separation between a Heavy PLF and a light NOF .

The primary NOF 's yield actually displays an exponential dependence with mass and charge, $Y(A) \sim \exp(-0.12A)$ and $Y(Z) \sim \exp(-0.32Z)$ as is seen from the semilogarithmic plots in figure 7, where the contributions from each impact parameter are summed up with the corresponding geometrical weight.

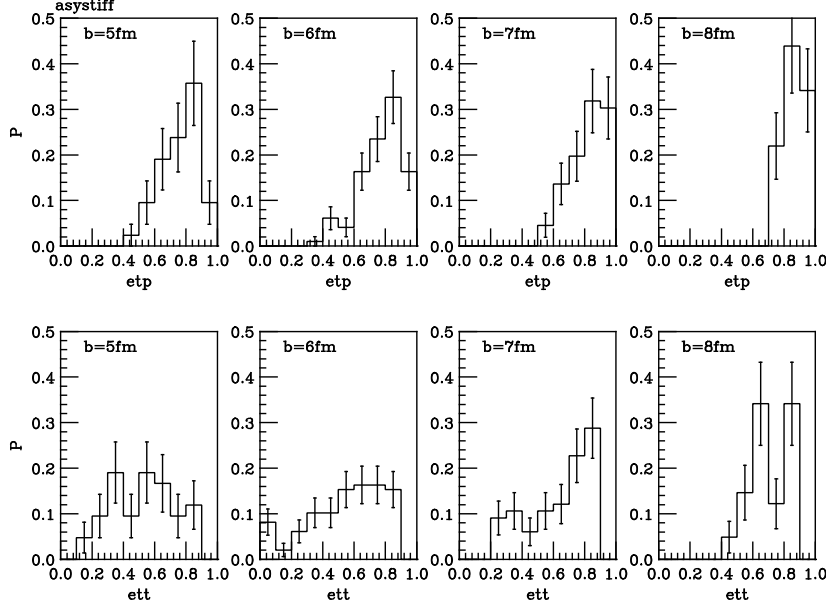


Fig. 6. Mass asymmetry $PLF - NOF$ (up) and $TLF - NOF$ (down) probability distribution for impact parameters from $b = 5fm$ to $8fm$ and asystiff EOS . Freeze-out times.

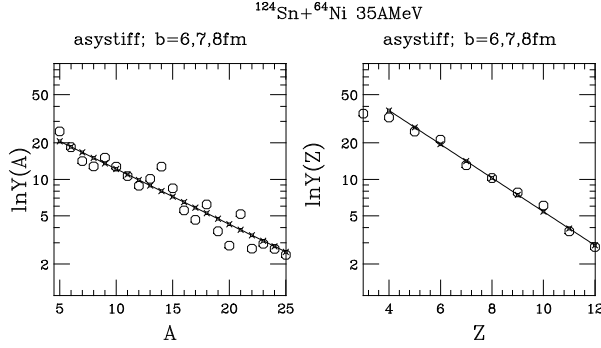


Fig. 7. Mass and charge distribution in neck fragmentation.

The values of slope parameters can depend on the constraints discussed before.

Finally for the same impact parameters the asymptotic fragment velocity distributions, in the laboratory frame, are plotted in Figure 8 both for binary and ternary events. Here ' v_{par} ' is the velocity component along the beam direction and ' v_{tran} ' is the orthogonal part. The NOF are found in relatively wide midrapidity region, close to the CM velocity which is around $5.4cm/ns$.

All these results guide us to individuate a fast neck break-up mechanism triggering the formation of an IMF , localized in the midvelocity region, the NOF . The emission take place in a temporal window between $140fm/c$ to $260fm/c$ from the reaction beginning. The best physical conditions are created at intermediate impact parameters, between $b = 5fm$ and $8fm$ for the

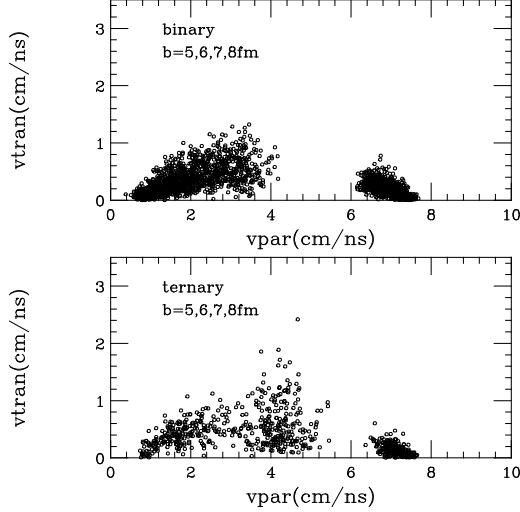


Fig. 8. Longitudinal and transversal velocity components of all fragments observed in binary events (up) and ternary events (down).

considered system. This is what we call *neck fragmentation mechanism*. Our task in the following sections is to study its particularities performing a more detailed analysis of *NOF*'s velocities and angular distributions as well as of their isospin content.

3 NECK FRAGMENTATION: KINEMATIC CORRELATIONS

In order to reveal the nonstatistical features of the *NOF* production we will look here at some clear kinematic correlations of dynamic nature. The corresponding observables can be promptly measured in exclusive experiments.

3.1 Deviations from Viola systematics

We first construct the asymptotic relative velocities of the neck-produced *IMFs* with respect to the *PLF* (*TLF*), $v_{rel}(PLF, TLF) \equiv |\mathbf{v}_{PLF, TLF} - \mathbf{v}_{NOF}|$. We compare these quantities to the relative velocities from a pure Coulombian driven separation, in a hypothetical statistical fission process of a compound *PL* or *TL* system, as provided by the Viola systematics [34,35]:

$$v_{viola}(1, 2) = \sqrt{\frac{2}{M_{red}} \left(0.755 \frac{Z_1 Z_2}{A_1^{1/3} + A_2^{1/3}} + 7.3 \right)} \quad (1)$$

were A_1, A_2, Z_1, Z_2 are the mass and charge number of the fission products and M_{red} is the corresponding reduced mass. We introduce the quantities

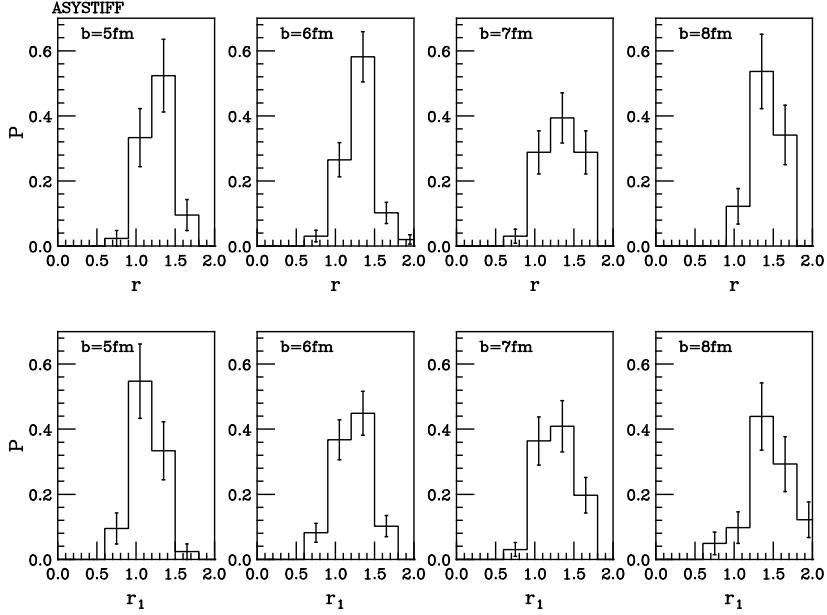


Fig. 9. Probability distributions of the deviations from Viola systematics with respect to *PLF* (r) (top) and *TLF* (r_1) (bottom) respectively. Impact parameters from $b = 5fm$ to $8fm$ and asystiff *EOS*.

$r(r_1)$, as the ratio between the observed *PLF*(*TLF*) – *NOF* relative velocity and the one obtained from Viola systematics, i.e. $r = v_{rel}(PLF)/v_{viola}(PLF)$, ($r_1 = v_{rel}(TLF)/v_{viola}(TLF)$). For each impact parameter, we calculate the r and r_1 probability distributions as shown in Figure 9. Most of them have relative velocities with respect to *PLF* (*TLF*) from 25% to 70% larger than the values provided by the Viola systematics. The distributions move towards larger deviations with increasing impact parameter.

It can be argued that a fragment showing a large deviation from Viola systematics with respect to the *PLF* is actually more correlated to the *TLF*, i.e. to a large r will correspond a closer to one r_1 and viceversa, a situation that will resemble more to a statistical fission scenario rather than to a dynamical production. We have tested this possibility plotting r_1 against r for each *NOF*, in Figure 10, [36]. The solid lines represent the locuses of the *PL*- ($r = 1$) and *TL*-fission ($r_1 = 1$) events respectively. The observed values (r, r_1) mostly appear simultaneously larger than one suggesting a weakened *NOF* correlation with *both PLF* and *TLF*, ruling out the statistical fission mechanism.

In some respect the process is more displaying an analogy with the participant-spectator scenario. However the dynamics appear much richer than in this simple sudden abrasion model, where the locus of the $r - r_1$ correlation should be on the bisectrix, apart the Goldhaber widths, see ref.[12]. Here we see wide distributions revealing a broad range of fragment velocities, typical of the instability evolutions in the neck region that will lead to large dynamical

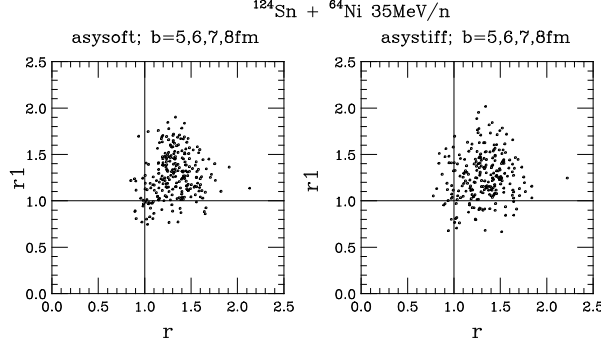


Fig. 10. Wilczynski-2 Plot: correlation between deviations from Viola systematics (see the text for definitions and ref.[36]). Results are shown for two *asy* – *EOS*.

fluctuations on *NOF* properties.

An induced asymmetric fission can also manifest some deviations from Viola systematics. In general, from our simulations, this mechanism takes place on longer time scales comparing to the neck fragmentation. In any case if a light fragment escapes later from its *PL*/*TL* partner, the friction certainly will attenuate the dynamical effects and relative velocities will deviate less from Coulomb contribution. In the plane $r - r1$ such events are located closer to the line $r = 1$ or $r1 = 1$. Moreover a prolonged *PL* or *TL* joint propagation will determine also different angular distributions in comparison to the neck fragmentation. This will be then another interesting correlation to look at. See the next point.

3.2 Narrow angular correlations around alignment

In the situation of a dynamically induced fission the reaction is expected to proceed as a two step process. Two primary excited fragments after a deep inelastic interaction, *PLF** and *TLF** are first produced. Their separation axis has direction and orientation given by the *PLF**-*TLF** relative velocity, $\mathbf{n}_S = (\mathbf{v}_{PLF^*} - \mathbf{v}_{TLF^*})$. The reaction plane is then defined by the normal vector constructed from the beam axis and separation axis as $\mathbf{n} = (\mathbf{n}_S \times \mathbf{n}_B)$, where $\mathbf{n}_B = \mathbf{v}_{CM}$. In this plane we introduce the z -axis along the beam direction and with the same orientation and the x -axis orthogonal to it and oriented from target to projectile.

In the second stage, depending on their excitation energy and deformations, the primary fragments can decay into the fission channel. Since in our case the projectile is heavier and more fissile we will consider the case of a *PLF* induced fission. The fission axis is determined by the relative velocity of fission products, denoted here as *H* (Heavy) and *L* (Light), to suggest an asymmetric process of interest for the comparison with our *IMF* production: $\mathbf{n}_F = (\mathbf{v}_H -$

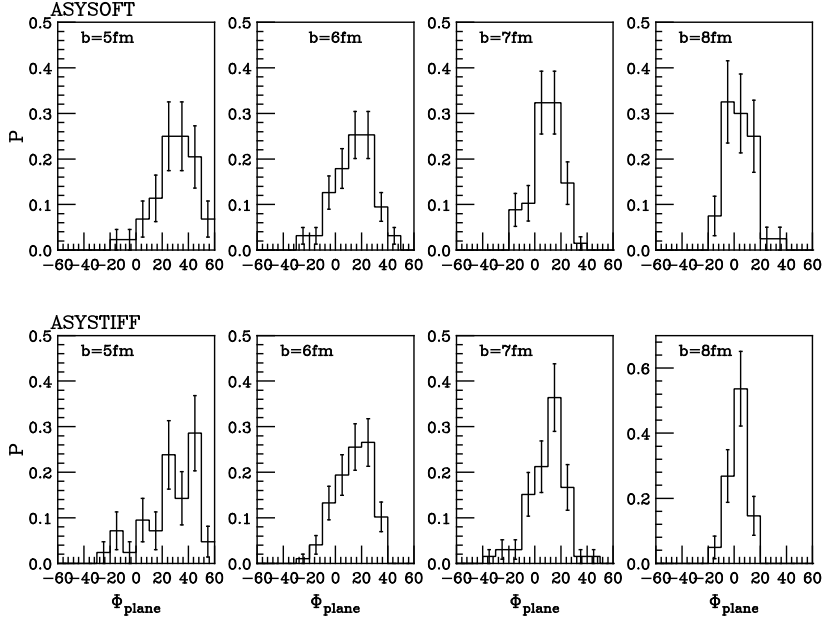


Fig. 11. The Φ_{plane} probability distributions: top, asysoft EOS, bottom, asystiff EOS. Impact parameter range from $b = 5fm$ to $8fm$.

\mathbf{v}_L). The in-plane azimuthal angle, Φ_{plane} , is the angle between the projection of the fission axis onto the reaction plane and the separation axis. We follow the convention introduced in [37], and consider the angle Φ_{plane} positive when $\mathbf{n}_S \times \mathbf{n}_F$ and \mathbf{n} both point into the same half-space. A $|\Phi_{plane}| \simeq 0$ collects events corresponding to asymmetric fissions of the PL -system very aligned along the outgoing $PL - TL$ separation axis. A statistical fission dominance should correspond to a flat Φ_{plane} distribution.

It is then instructive, as we will see, to adopt the same language and system of definitions when studying the angular correlations in the neck fragmentation mechanism. The Φ_{plane} distributions, corresponding to the same NOF events analysed before, are shown in figure 11 for impact parameters from $b = 5fm$ to $8fm$ and two *asy*-EOS, asysoft and asystiff. The NOF 's are observed in a quite limited angular window, close to full alignment configurations, $\Phi_{plane} = 0^\circ$. The range of values $\Delta\Phi_{plane} \approx 80^\circ$ for $b = 5fm$ is becoming narrower with increasing impact parameter. However the angular distributions are not symmetrically distributed around $\Phi_{plane} = 0^\circ$, but shifted toward positive values. This behavior is more evident at smaller impact parameters but even at $b = 8fm$ for more than 60 – 65% of ternary events Φ_{plane} is positive. These properties reflect entrance channel effects and early stages of the neck fragmentation dynamics and NOF formation.

Indeed, this can be clearly realized from the figure 12 were we plot the freeze-out CM velocity components v_z and v_x , of all fragments identified in the ternary events. We can easily localize the PLF 's and TLF 's positions. Their x -

component velocities reflect the orbiting motion before separation (see Figs.2, 3). The freeze-out v_z 's, when compared to the corresponding initial velocities in the CM , are an indication of the kinetic energy dissipation.

Most of the NOF 's have their CM velocity components v_z, v_x both negative. This is a consequence of their early decoupling combined to the Coulomb repulsion. A simple analysis upon these velocity distributions indicates that the corresponding Φ_{plane} angle has to be quite small and positive as it was seen in the previous figure. The fast neck-fragmentation mechanism is essential to understand this behavior, in particular if we look at the third quadrant points which are well off the rotational axis connecting the TL and PL velocity regions. Here if only Coulombian effects are manifest v_x has to be anticorrelated with v_z : if moving counterclockwise, v_x should decrease in absolute value meanwhile the modulus of v_z will increase. We do not see this correlation: rather they look proportional. This can be associated with the collective expansion of the neck matter on the way toward separation, between $60fm/c$ and $160fm/c$, which, because of geometrical configuration (see also Fig.2) will enhance mainly the negative x -component of the fragment velocity.

This is a new dynamical effect which adds its contribution to the observed deviations from Viola systematics. Indeed, a NOF , depending on the time and place where is formed, will experience in a certain degree this collective motion. From Fig.12 we can see that for $b = 5, 6, 7fm$ (v_z, v_x) can reach values up to $(-2cm/ns, -1cm/ns)$. The IMF 's with largest negative v_x components (and largest positive Φ_{plane} angles) represent the earliest fragment formation in the neck region: they should show the lowest correlation to the PL residues. If this is true then we expect that the deviation from Viola systematics has a rising trend when moving toward positive Φ_{plane} angles. The value of Φ_{plane} for which this maximum is attained as well as corresponding value of maximum are directly related to the dynamical effect just discussed. Beside this we have to add that, less frequently in this mass asymmetric system, the fast NOF 's can be formed also on the other side of the neck and so they will experience an enhancement of v_x in positive direction. Since in this case Φ_{plane} is negative, we expect some rise of the *Viola - violation* r -parameter, more discrete, also at negative angles. This features are indeed observed when we look at the correlation with the Projectile-like system $\Phi_{plane} - r$ in figure 13. We note that this mechanism naturally predicts a dip in the r -values in correspondence to the $|\Phi_{plane}| \simeq 0$ region, i.e. for PLF breakings fully aligned along the separation axis.

When the light fragment remains attached longer to the heavy one, the Φ_{plane} distribution becomes flatter and the deviation from Viola systematics diminishes gradually. However, as mentioned before, it is hard to follow this process (the dynamical fission) within BUU-like approaches.

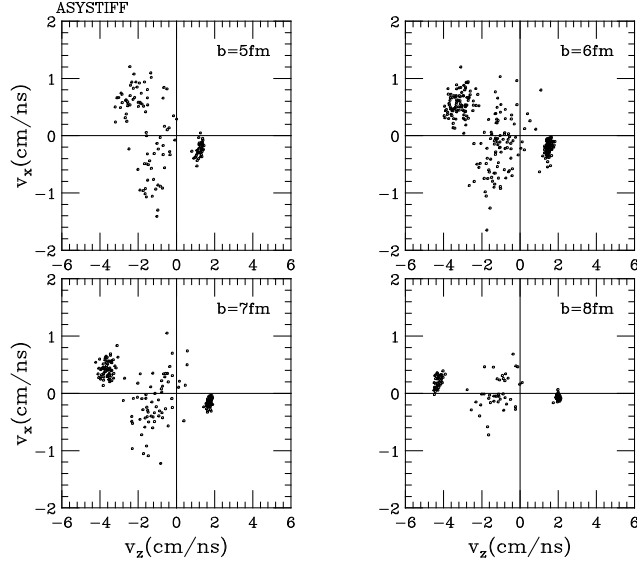


Fig. 12. Center of mass z, x -velocity components distributions.

Summarizing this discussion, we conclude that the Φ_{plane} angle is a very appropriate observable to disentangle among various mechanisms. For the asymmetric reaction considered here, an anisotropic distribution, populating preferentially positive small angles, but extended also at negative angles, characterize neck fragmentation mechanism. The largest deviations from Viola systematics due to neck expansion will be reached at positive angles. An induced dynamical fission, expected as the next fast process in a temporal ordering, will be characterized by a wider but still anisotropic distribution and by smaller deviations from Viola systematics. Finally, closer to a statistical fission, large angles, in absolute values, can also be reached. Meanwhile more events with mass symmetric *PLF* fission will appear. The Heavy/Light mass ratio A_H/A_L appears then also a good parameter to select fast neck-dynamics effects.

4 UNVEILING THE NECK FRAGMENTATION MECHANISM: ROLE OF VOLUME INSTABILITIES

The results presented in the previous sections were obtained considering a free, energy dependent nucleon-nucleon cross sections and a soft *EOS* parametrization with a compressibility modulus around 200 MeV.

In the Fermi energy domain the mean-field and the two-body collisions have comparable effects on the dynamical evolution. A classical example is provided by the collective flows: none of the two ingredients, alone, can reproduce the observed experimental behaviour. Here we are concerned with their influence on the neck fragmentation dynamics.

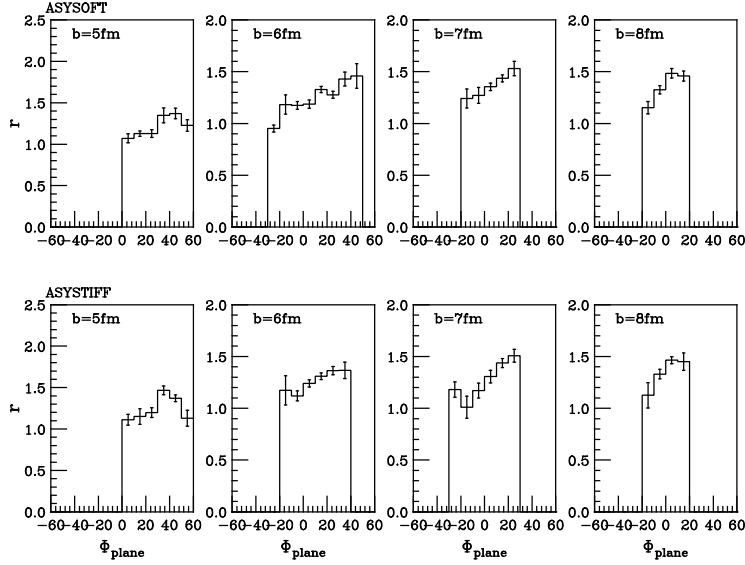


Fig. 13. Φ_{plane} angle dependence of the deviation from Viola systematics.

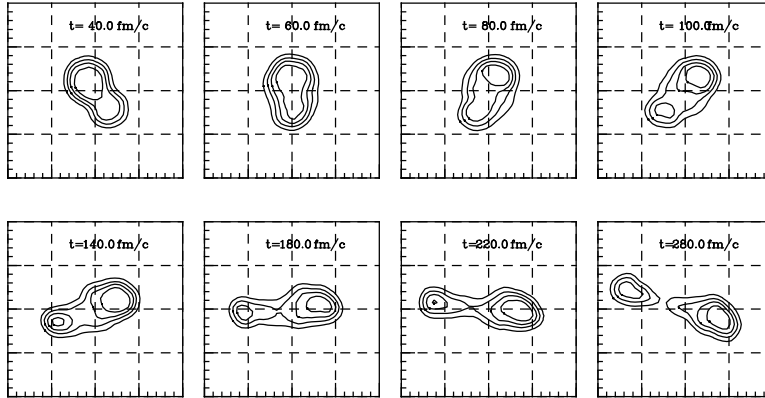


Fig. 14. Typical evolution of density contour plot for a $b = 6fm$ event simulation with a hard EOS .

4.1 EOS dependence

We first perform new simulations adopting a hard, ($K = 380MeV$), equation of state and keeping unchanged the nucleon-nucleon cross-sections. We have run 400 events at a chosen impact parameter $b = 6fm$, for which, with the soft mean field the neck fragmentation had the most frequent appearance. During the first $300fm/c$ no ternary event was observed. From density contour plots, like Figure 14, a quite different evolution is apparent.

A more consistent neck will bind PL and TL prefragments longer time together. Moreover, no evident decoupling of the participant region is manifest. Rather, the separation takes place by the rupture of a very elongated neck structure.

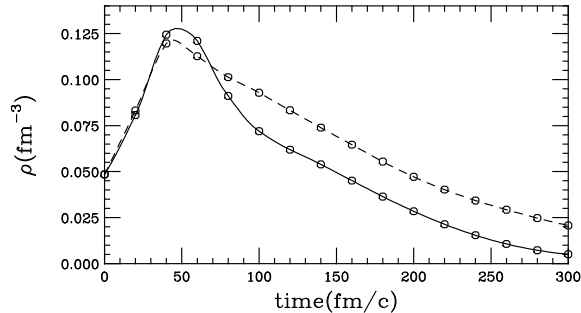


Fig. 15. Density evolution in the neck region (see the text) for soft *EOS* ($K=200\text{MeV}$, solid) and stiff *EOS* ($K=380\text{MeV}$, dashed).

This new reaction evolution must be related to the different bulk compression-expansion dynamics. In order to clarify this point, in Fig.15 we plot the time evolution of the average nuclear matter density in a cubic volume of 10fm side, centered in the *CM*, in the two cases. With a soft *EOS* (solid line) we see a large initial density oscillation. The neck zone will deeply enter the low density spinodal instability region with a fast cluster formation on a time scale comparable with the *PLF* – *TLF* separation time due to the rotation. This will lead to the observed early *NOF* decoupling from moving *PL* and *TL* prefragments. The growth time of density instabilities is also in agreement with the observation that fragments appear after $140\text{fm}/c$ [38].

With a hard *EOS* (dashed line) the density oscillation is much reduced, the neck-system is hardly entering the dilute unstable region. Instabilities, if any, will grow on a very long time scale and the neck will break before any *PLF/TLF*-decoupled cluster formation.

The geometrical and temporal constraints will limit the size of the formed *NOF*'s, setting an important difference with respect to the spinodal decomposition in multifragmentation processes, [39], [25], where it was involved as the kinetic process that initiates the fragment formation.

Nevertheless the surface fluctuations in the neck region may play also a role in causing the density inhomogeneities. Our results seem to show that the volume contributions are essential and *NOF* multiplicities will be sensitive to the *EOS* stiffness.

4.2 Influence of the *NN* cross sections

Two-body collisions prove also to be important in the dynamics of this mechanism. We have performed a new set of calculations, with a soft *EOS* but reducing to a half the values of nucleon-nucleon cross sections. Quite puzzling, the number of ternary events is increasing by a factor two over all the

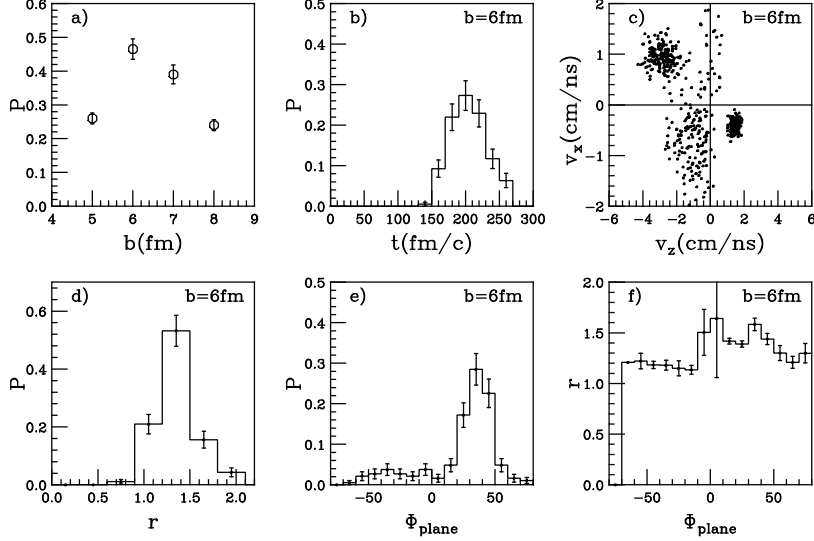


Fig. 16. Main features of neck fragmentation simulations with reduced NN cross sections (see text).

range of impact parameters, see Figure 16 a). We even noticed events with emission of two NOF s, around 10% of the total.

The NOF formation is somehow anticipated. We observe earlier high production rates, see for comparison, the Figures 16 b) and 5. The highest rates, for $b = 6fm$, are now attained between $180fm/c$ and $230fm/c$ meanwhile previously the maximum was between $200fm/c$ and $250fm/c$.

The NOF 's v_z velocity components are not much affected by the cross sections reduction while a definite influence is observed on the transversal components v_x , which now, for $b = 6fm$, extend from $-2cm/ns$ to $2cm/ns$, as can be seen from Fig. 16 c). This behaviour, in conjunction to the fact that PLF velocities are less damped, has as a direct consequence some larger deviations from Viola systematics, see Fig. 16 d), and a shift of the Φ_{plane} distribution toward larger positive values, Fig. 16 e).

We remind that the collisional friction is essential for the midrapidity stopping power, the warm and dense neck zone formation and the dynamical fluctuations which originate from the instabilities. The presented results show that the tuning of the collisional contribution also modifies the neck separation dynamics. Reduced NN cross sections will favour the instabilities development. Moreover, owing to a smaller stopping, the neck-breaking time is better matching the time scales of the instabilities that lead to a NOF formation. The characteristics of the process, NOF 's emission probability, angular distributions and deviations from Viola systematics, are consequently clearly affected.

5 THE ISOSPIN DYNAMICS IN NECK FRAGMENTATION

From the results shown in the previous sections we can notice that the symmetry term of EOS does not influence sensitively the main pattern of the neck fragmentation mechanism: probability of ternary events, deviations from Viola systematics and NOF angular distributions. We have to say that with the studied system we cannot reach high charge asymmetries, the asymmetry parameter $I \equiv (N - Z)/A$ ranging from 0.193 for the projectile and 0.125 for the target to an average $I = 0.17$.

However we will show in this section that we can clearly select other quantities, as average isospin content of fragments or isotopic probability distributions, that appear much more sensitive to the symmetry energy term. In other words observables that are widely related to the isospin diffusion during the neck dynamics appear more sensitive to transport properties of the effective interaction in the isovector channel.

On the other hand we have concluded that neck fragmentation is a quite fast mechanism, driven by dynamical effects in the first $150fm/c$ - $300fm/c$, depending on the impact parameter. Therefore it can provide distinct conditions for studying the isospin dynamics on various time scale. Moreover, due to density variations in the neck regions, we hope that in this way we could directly test the density dependence of the symmetry potential.

5.1 Isospin dynamics

For the three *asy* - EOS introduced in Section 2 we plot in the Fig.17 the average isotopic composition I of the NOF 's as a function of the PLF r -deviation from Viola systematics. At all impact parameters clear differences are evidenced. The average asymmetry does not depend strongly on r . We notice however that it increases proportionally with the slope of the symmetry potential as a function of density around and below normal density. The *supersystiff* parametrization, i.e. with an almost parabolic increasing behavior around ρ_0 , produces sistematically more neutron rich NOF 's.

This effect is clearly due to a different neutron/proton migration at the interface between PL/TL "spectator" zone around normal density and the dilute neck region where the NOF 's are formed. In order to understand the details of this isospin diffusion dynamics we follow the time evolution of the average density and average asymmetry in the spatial cubic volume of $10fm$ side around the CM introduced in the previous section and containing mainly the neck zone. The corresponding correlation is shown in Fig.18 for *asysoft* and *supersystiff* parametrizations. The numbers close to the each symbol indicate

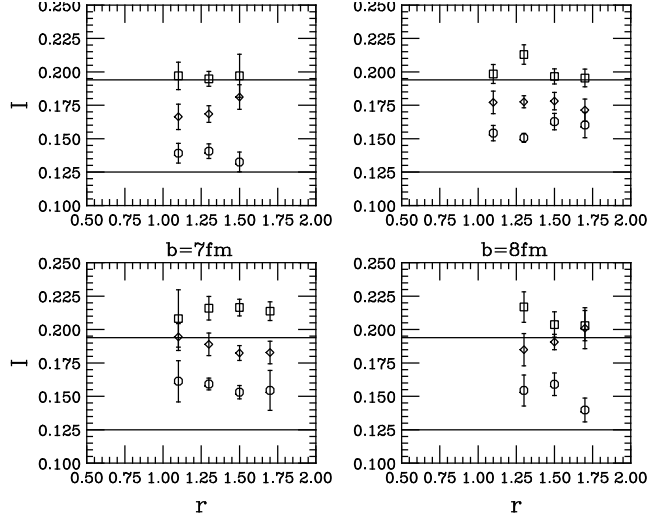


Fig. 17. *NOF* isospin content for *asysoft* (circles), *asystiff* (rombs) and *superasystiff* (squares) *EOS* as a function of *r*-deviation from Viola systematics, at impact parameters from $b = 5fm$ to $8fm$. The two solid lines represent the mean asymmetries of the projectile (top) and target (bottom).

the corresponding time step.

The density variations in the considered volume are very similar for the two *asy* – *EOS*, at each time the circle and square points are aligned roughly at the same mean density ρ . This is not surprising since the density oscillations are due to the stiffness of the symmetric (isoscalar) part of the *EOS* which is kept exactly the same (soft choice here) for the two different *asy* – *EOS* parametrizations. Actually the overall compressibility in asymmetric matter is modified by the density dependence of the symmetry term, see [30], but the effect is not large and proportional to the square of the mean asymmetry I . This can explain the very tiny alignment shift between circles and squares in Fig.18.

The initial average asymmetries have values close to that of the composite system ($I = 0.17$). The differences until $80fm/c$ can be assigned to a different relative fast neutron to proton emission from the central region. In this time interval we have a density oscillation, see Fig.15, and so neutrons are probing some more mean field repulsion in the superasystiff case (the circles slightly below the squares).

After $80fm/c$ the dilute neck region is forming, see Fig.2, and a clear dependence on the used *asy* – *EOS* of the isospin dynamics is evident. A much larger neutron enrichment of the neck zone for the asysuperstiff *EOS* takes place. We can understand this results in simple terms. In presence of density and isospin gradients, as in the case of neck fragmentation, the nucleons will feel the superposed effects of the forces due to the isoscalar and isovector part of the mean field. In the asysuperstiff case the neutrons will be accelerated

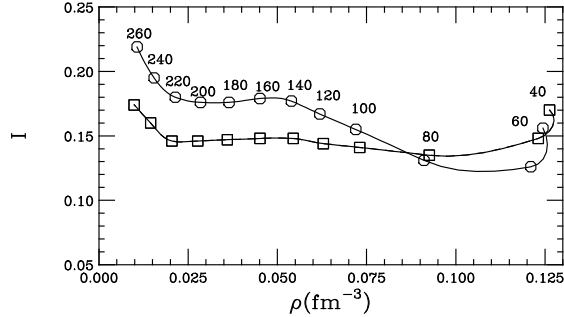


Fig. 18. Mean asymmetry-density correlations in a cubic volume centered around the CM during the reaction evolution, see the text. The points are obtained by averaging over all events for asysoft (squares) and superasystiff (circles) EOS at $b = 6fm$.

towards the neck region since the repulsion of the symmetry part of the mean field is sharply increasing around normal density. This migration from spectator to neck at the interface compensates in part the neutrons that moves out from the participant region in presence of the expansion causing finally the observed enrichment. This effect is largely reduced in the asysoft case due to the flatness of the density dependence of the symmetry mean field around ρ_0 .

This trend is not modified when reducing by half the nucleon-nucleon cross-sections. The reason is related to the fact that at these energies, and lower densities, we are concerned with a transport regime intermediate between ballistic and hydrodynamical.

From the last two figures we see that the isospin content of NOF 's carries important information on the isovector part of the effective interaction and the related isospin dynamics in the early stages of the reaction. We expect a different isospin pattern for the IMF 's resulting from induced and/or statistical fission of the more charge symmetric PLf^* 's and TLF^* 's.

5.2 Isoscaling

In recent years interesting isospin effects on fragment production were evidenced through a isoscaling behaviour, observed first in multifragmentation [40,41]. It was experimentally observed that when compared two different reactions, one neutron rich (label 2) and the one neutron poor (label 1), the ratio between the corresponding yields of a given N, Z isotope $R_{21} = Y_2(N, Z)/Y_1(N, Z)$ verifies the following relation:

$$\ln R_{21} = Cost + N\alpha + Z\beta \quad (2)$$

with α and β isoscaling parameters. In a grand-canonical statistical approach these parameters are related to the neutron (proton) chemical potential differences between the nuclear environments where the fragments are created in the two reactions:

$$\alpha \equiv \frac{\Delta\mu_n}{T} \quad , \quad \beta \equiv \frac{\Delta\mu_p}{T} \quad , \quad (3)$$

In turn, these are related to the symmetry energy properties:

$$\begin{aligned} \Delta\mu_n &= \rho \frac{\partial E_{sym}}{\partial \rho} (I_2^2 - I_1^2) + 2E_{sym} [(I_2 - I_1) - \frac{(I_2^2 - I_1^2)}{2}] \\ \Delta\mu_p &= \rho \frac{\partial E_{sym}}{\partial \rho} (I_2^2 - I_1^2) - 2E_{sym} [(I_2 - I_1) + \frac{(I_2^2 - I_1^2)}{2}] \end{aligned}$$

where E_{sym} is defined by

$$E(\rho, I) \equiv \frac{\epsilon(\rho, I)}{\rho} = E(\rho) + E_{sym}(\rho)I^2 + O(I^4) + \dots \quad (4)$$

$$|\Delta\mu_p| < |\Delta\mu_n|.$$

Since always we have the following relation:

$$\ln \left(\frac{N_2/Z_2}{N_1/Z_1} \right) \equiv \alpha - \beta = \frac{4}{T} E_{sym}(\rho) (I_2 - I_1) \quad (5)$$

a large interest is rising on the possibility of a direct measurement of the symmetry energy in the fragment source from the isoscaling α, β parameters.

We have tested if the isoscaling behavior can manifest in neck fragmentation too, when characteristic time scales are shorter and several dynamical features will make questionable the previous statistical equilibrium arguments. To this purpose we have performed the same calculations for the neutron-poor $^{112}\text{Sn} + ^{58}\text{Ni}$, accumulating the same “statistics”, 400 events for each $b = 6, 7, 8\text{fm}$ impact parameter.

In figures 19, (20) are shown the N (Z) dependence of $\ln R_{21}$, for $Z = 1$ to $Z = 9$ light fragments produced in the neck region, as obtained from our calculations for a *asystiff* – *EOS* parametrisation:

We clearly see a nice isoscaling signal, exponential N - and Z - dependence of the yield ratios with very well defined α, β slopes. All that in spite of the dynamical features of these *NOFs* that we have extensively described in the previous sections.

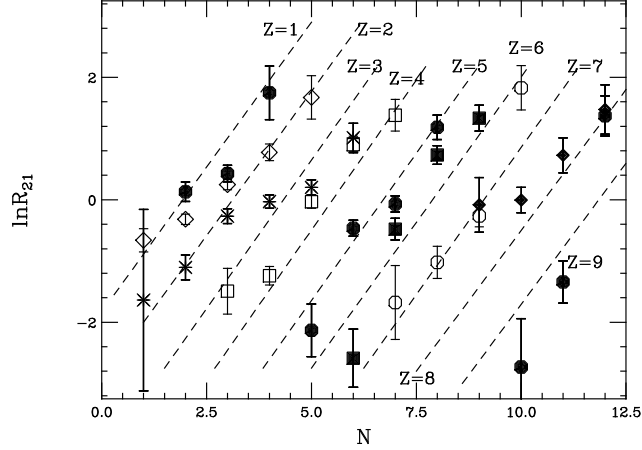


Fig. 19. Isoscaling in neck fragmentation: $\ln R_{21}$ dependence on N .

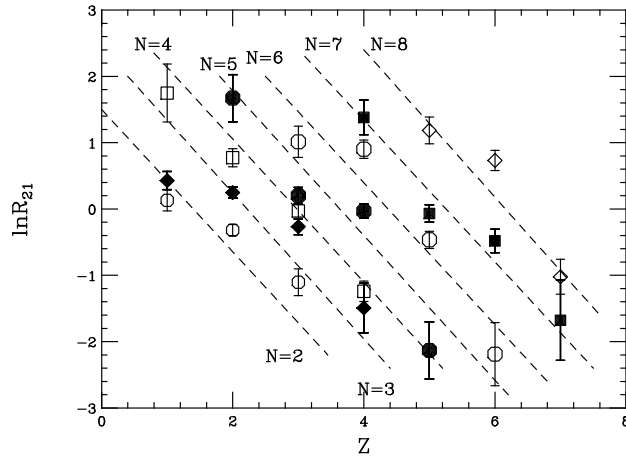


Fig. 20. Isoscaling in neck fragmentation: $\ln R_{21}$ dependence on Z .

Although we cannot use explicit equilibrium relations, like Eq.5, we still expect a symmetry energy dependence of the isoscaling parameters. Since the fragment formation takes place in the neck region, we can predict that its isospin content will dictate the values of the isoscaling parameters. Indeed we may assume that for a neutron poor system, closer to symmetric case, the differences between various *asy* – *EOS* on the isotopic and isotonic distributions are reduced, and in a first approximation identical. At variance, for neutron rich system, by passing from *asysoft*- to *superasytiff*-*EOS*, we have seen that a more neutron-rich neck region is forming, favorating a relative larger production of more asymmetric *IMF*'s. Therefore, the corresponding distributions have to be steeper.

We have then repeated all the calculations for the three different *ASY* – *EOS* and we see, as reported in Table I, a nice increase (modulus) of the isoscaling parameters with the increasing stiffness of the symmetry energy.

	<i>asysoft</i>	<i>asystiff</i>	<i>superasystiff</i>
α	0.69	0.95	1.05
β	-0.67	-1.07	-1.18

Table 1

The isoscaling parameters α and β in neck fragmentation for three asy-EOS.

We can summarize, saying that neck fragmentation mechanism, owing to its particular features, can provide distinct opportunities to study the density dependence of *asy* – *EOS*.

6 CONCLUSIONS

In the framework of a microscopic transport model, based on a stochastic extension of the *BNV* equation, we investigate the “dynamical” *IMF* production observed experimentally in semicentral heavy ion collisions in the Fermi energy domain. For the reaction $^{124}\text{Sn} + ^{64}\text{Ni}$, we identify two main mechanisms responsible for the *IMF* emission that cannot be ascribed to the statistical decay of *PLF* or *TLF*: a neck fragmentation mechanism, a fast process, that takes place within first $200\text{fm}/c$ to $300\text{fm}/c$ and the dynamically induced fission, triggered by the large deformations acquired during the interaction stage, that we observe, in some events, at larger times.

We have studied in detail the features of neck fragmentation, as a source of *IMF* emission in the midrapidity region.

This *IMF* emission appears largely decorrelated to *PLF* or *TLF* statistical emission. Indeed the relative asymptotic velocities *IMF* – *PL(TL)F* show deviations from the Viola systematics ranging from 25% to 70%. We interpret this as the consequence of an early decoupling of the neck zone, where the *IMF*’s are formed, from the *PLF* and *TLF*. Indeed, at the separation time, because of incomplete dissipation of their collective motion, *PL* and *TL* residues have relative velocities, with respect to the participant region, well above the values associated with a pure Coulomb repulsion.

We observe that the neck region, due to expansion effects, as well as to the contemporary *PLF*-*TLF* centrifugal motion is quenched inside the spinodal instability region. Hence we identify the spinodal decomposition as the kinetic process driving fragment formation in the neck region. As a consequence, we find that the mean field compressibility is governing the neck fragmentation dynamics, while the nucleon-nucleon cross section value shapes its properties.

Results regarding the *NOF*’s kinematical properties are in qualitative agree-

ment with the experimental observations. We can also underline that a proper confrontation of these events with the transport model predictions can impose new constraints on the in medium nucleon-nucleon cross sections.

We observe interesting effects in the isospin dynamics, related to the density and asymmetry gradients between participant and spectator regions. The neck region becomes more charge asymmetric due to neutron migration, a process influenced by the asy-EOS density dependence. We show that the effect is more pronounced for larger slopes of the symmetry energy around and below saturation density values. The IMF isospin content keeps track of this early neutron enrichment process.

Predictions are in agreement with the experimental observations, based on isotopic distributions of light particles, of a neutron richer neck zone. Interesting enough, we observe isoscaling in the neck fragmentation, inspite of the short time scales of the IMF production. The isoscaling parameters, α and β , are sensitive to the density dependence of the asy-EOS, increasing in absolute values when going from asy-soft to asy-stiffer EOS.

Acknowledgements

We warmly thank the *CHIMERA – REVERSE* Collaboration for the continuous exchange of information on their data analysis. In particular we are very grateful for the stimulating discussions with Janusz Wilczynski, Eric Piacsek, Angelo Pagano and Enrico De Filippo.

References

- [1] C.P. Montoya et. al.: Phys.Rev.Lett. **73** 3070 (1994).
- [2] J. Toke et. al.: Phys.Rev.Lett. **75**, 2920 (1995).
- [3] J. Lukasik et al.: Phys. Rev. **C 55**, 1906 (1997).
- [4] L.G. Sobotka et al.: Phys. Rev. **C 55**, 2109 (1997).
- [5] F. Bocage et al.: Nucl. Phys. **A 676**, 391 (2000).
- [6] T. Lefort et al.: Nucl. Phys. **A 662**, 397 (2000).
- [7] P. M. Milazzo et al.: Phys. Lett. **B 509**, 204 (2001).
- [8] P. M. Milazzo et al.: Nucl. Phys. **A 703**, 466 (2002).
- [9] B. Davin et al.: Phys. Rev. **C 65**, 064614 (2002).
- [10] S. Piantelli et al.: Phys. Rev.Lett. **C 885**, 052701 (2002).
- [11] J. Colin et al.: Phys. Rev. **C 67**, 064603 (2003).
- [12] J. Lukasik et al.: Phys. Lett. **B 566**, 76 (2003).
- [13] A.S. Botvina et al.: Phys. Rev. **C 59**, 3444 (1999).
- [14] M.Colonna, M.Di Toro, A.Guarnera: Nucl.Phys. **A589**, 160 (1995).
- [15] J. F. Dempsey et al.: Phys. Rev. **C 54**, 1710 (1996).
- [16] U. Brosa, S. Grossman, A. Muller: Phys. Rep. **197**, 167 (1990).
- [17] G. Poggi: Nucl. Phys. **A 685**, 296C (2001).
- [18] D. J. Rowland et al.: Phys. Rev. **C 67**, 064602 (2003).
- [19] G. A. Souliotis et al.: Phys. Rev. Lett **91**, 022701 (2003).
- [20] G. A. Souliotis et al.: Phys. Rev. **C 68**, 024605 (2003).
- [21] M. B. Tsang: Nucl. Phys. **A 722**, 136c (2002).
- [22] B.Jonson et al.: *EURISOL Proposal, Key Experiments Task Group*, Final Report, 2003. On the web site “www.ganil.fr/eurisol/”.
- [23] A. Pagano et al.: Nucl. Phys. **A 681**, 331c (2001).
- [24] M.Colonna et al.: Nucl.Phys. **A 642**, 449 (1998).
- [25] A. Guarnera et al.: Phys. Lett. **B 373**, 267 (1996).
- [26] V. Greco, A. Guarnera, M. Colonna, M. Di Toro: Phys. Rev. **C 59**, 810 (1999).
- [27] M. Colonna et al.: Phys. Rev. **C 47**, 1395 (1993).

- [28] M.Colonna et al.: Nucl.Phys. **A 580**, 312 (1994).
- [29] V.Baran et al.: Nucl.Phys. **A 703**, 603 (2002).
- [30] M. Di Toro et al.: Prog. Part. Nucl. Phys. **42**, 125 (1999).
- [31] M. Prakash et al.: Phys. Rep. **280**, (1997).
- [32] Bao-An Li: Phys. Rev. Lett. **85**, 4221 (2000).
- [33] G.J. Kunde et al.: Phys. Rev. Lett. **77**, 2897 (1996).
- [34] V. Viola et al.: Phys. Rev. **C 31**, 1550 (1985).
- [35] D.J. Hinde et al.: Nucl. Phys. **A 472**, 318 (1987).
- [36] We like to call the $r - r_1$ -correlation plot as *Wilczynski-2 Plot*. Indeed this correlation, very important to rule-out a statistical fission scenario for fragments produced at mid-rapidity, nicely emerged during hot discussions with Janusz Wilczynski at the *LNS - INFN*, Catania.
- [37] A.A. Stefanini et al.: Z. Phys. **A 351**, 167 (1995)
- [38] V.Baran, M.Colonna, M.Di Toro, A.B. Larionov: Nucl.Phys. **A632**, 287 (1998).
- [39] M.Colonna, P. Chomaz: Phys.Rev. **C 49**, 1908 (1994).
- [40] H. S. Xu et al.: Phys. Rev. Lett. **85**, 716 (2000).
- [41] M. B. Tsang et al.: Phys. Rev. Lett. **86**, 5023 (2001).